Inorg. Chem. **2004**, *43*, 1379–1387

$[(NH_3)_5Ru(1,2,4,5\text{-tetrazine})]^{2+}$: Synthesis and Experimental and Theoretical Study of Its Solvatochromism in the Visible Spectral Region

Ivo Cacelli,[†] Silvio Campanile,[‡] Gianfranco Denti,*[,||] Alessandro Ferretti,*[,‡] and Milena Sommovigo[||]

Dipartimento di Chimica e Chimica Industriale, Università di Pisa, Via Risorgimento 35, Pisa, Italy, Istituto per i Processi Chimico-Fisici del CNR, Area della Ricerca, Via G. Moruzzi 1, I-56010 Pisa, Italy, and Dipartimento di Chimica e Biotecnologie Agrarie, Università di Pisa, Via del Borghetto 80, I-56124 Pisa, Italy

Received July 8, 2003

The title compound has been first synthesized and fully characterized as both tetraphenylborate and perchlorate salt. Its 300–900 nm absorption spectrum, recorded in nitromethane, water, and dimethyl sulfoxide, reveals the peculiar existence of two distinct bands whose intensities depend on the solvent donor number. This feature can be attributed to two separate metal-to-ligand charge-transfer transitions, in agreement with the theoretical predictions obtained by extensive configuration interaction calculations, which take into account the solvent effects. The calculation of the potential energy curves of the ground and excited states along the Ru–tetrazine coordinate allows the interpretation of the relative intensities of the observed bands, as well as the interpretation of their line-shape profiles.

Introduction

In the past decade, mono- and oligonuclear transition-metal complexes have attracted a large interest as materials for molecular electronics because of their remarkable nonlinear optical,[1] magnetic,[2] and electric[3] properties. Furthermore, they are envisaged as useful devices for quantum computing[4] and molecular memories,[5] likewise for organic polymers whose usefulness has been already proven.[6] Within this frame, a significant role is played by oligonuclear Ru and Os polypyridine complexes,[5b,7] in which a suitable choice of the bridging ligands can appropriately tune the metal−metal interaction.[8] Oligonuclear systems are known that contain as bridging ligands either bis-monodentate or bis-chelating molecules.[1c−e,5a] Classical mixed-valence compounds,[9] e.g., the well-known Creutz−Taube ion[10] $[(NH_3)_5Ru(\mu\text{-pyrazine})Ru(NH_3)_5]^{5+}$, belong to the first family of complexes.

In all of these species, the bridging ligand plays a central role in setting the properties connected to the intramolecular electron-transfer process. Thus, different bridging ligands having π and/or π^* orbitals well-delocalized over the whole

* Authors to whom correspondence should be addressed. E-mail: gdenti@agr.unpi.it (G.D.); ferretti@ipcf.cnr.it (A.F.).
[†] Dipartimento di Chimica e Chimica Industriale, Università di Pisa.
[‡] Istituto per i Processi Chimico-Fisici del CNR.
[||] Dipartimento di Chimica e Biotecnologie Agrarie, Università di Pisa.

(1) (a) Prasad, P. N.; Williams, D. J. *Introduction to Nonlinear Optical Effects in Molecules & Polymers*; John Wiley & Sons: New York, 1991. (b) Karna, S. P., Yeates, A. T., Eds. *Nonlinear Optical Materials: Theory and Modelling*; ACS Symposium Series 628; American Chemical Society: Washington, DC, 1996. (c) Ferretti, A.; Lami, A.; Villani, G. *J. Phys. Chem.* **1997**, *101*, 9439. (d) Sheadi, I. A.; Murga, L. F.; Ondrechen, M. J.; Lindergerg, J. *Chem. Phys. Lett.* **1998**, *291*, 325. (e) Di Bella, S. *Chem. Soc. Rev.* **2001**, *30*, 355.
(2) Kahn, O. *Molecular Magnetism*; VCH: New York, 1993.
(3) (a) Hanack, M.; Deger, S.; Lange, A. *Coord. Chem. Rev.* **1988**, *83*, 115. (b) Hanack, M. *Mol. Cryst. Liq. Cryst.* **1988**, *160*, 133. (c) Hanack, M.; Lang, M. *Adv. Mater.* **1994**, *6*, 819. (d) Mendizabal, F. *J. Mol. Struct.* **2001**, *579*, 169.
(4) Braun-Sand, S. B.; Wiest, O. *J. Phys. Chem. A* **2003**, *107*, 285.
(5) (a) Tomita, A.; Sano, M. *Inorg. Chem.* **2000**, *39*, 200. (b) Tyson, D. S.; Bignozzi, C. A.; Castellano, F. N. *J. Am. Chem. Soc.* **2002**, *124*, 4562.
(6) (a) Reed, M. A.; Chen, J.; Rawlett, A. M.; Price, D. W.; Tour, J. M. *Appl. Phys. Lett.* **2001**, *78*, 3735. (b) Fan, F.-R. F.; Yang, J.; Dirk, S. M.; Price, D. W.; Kosynkin, D.; Tour, J. M.; Bard, A. J. *J. Am. Chem. Soc.* **2001**, *123*, 2454. (c) Fan, F.-R. F.; Yang, J.; Cai, L.; Price, D. W.; Dirk, S. M.; Kosynkin, D.; Yao, Y.; Rawlett, J. M.; Tour, J. M.; Bard, A. J. *J. Am. Chem. Soc.* **2002**, *124*, 5550.
(7) (a) Balzani, V.; Campagna, S.; Denti, G.; Juris, A.; Serroni, S.; Venturi, M. *Acc. Chem. Res.* **1998**, *31*, 26. (b) De Cola, L.; Belser, P. *Coord. Chem. Rev.* **1998**, *177*, 301. (c) Barigelletti, F.; Flamigni, L. *Chem. Soc. Rev.* **2000**, *29*, 1.
(8) Di Pietro, C.; Serroni, S.; Campagna, S.; Gandolfi, M. T.; Ballardini, R.; Fanni, S.; Browne, W. R.; Vos, J. G. *Inorg. Chem.* **2002**, *41*, 2871.
(9) (a) Creutz, C. *Prog. Inorg. Chem.* **1983**, *30*, 1. (b) Crutchley, R. J. *Adv. Inorg. Chem.* **1994**, *41*, 273. (c) Endicott, J. F.; Watzky, M. A.; Song, X.; Buranda, T. *Coord. Chem. Rev.* **1997**, *159*, 295. (d) Kaim, W.; Klein, A.; Glöckle, M. *Acc. Chem. Res.* **2000**, *33*, 755. (e) Demadis, K. D.; Hartshorn, C. M.; Meyer, T. J. *Chem. Rev.* **2001**, *101*, 2655. (f) Launay, J.-P. *Chem. Soc. Rev.* **2001**, *30*, 386.
(10) Creutz, C.; Taube, H. *J. Am. Chem. Soc.* **1969**, *91*, 3988.

10.1021/ic034786o CCC: $27.50
Published on Web 01/24/2004

molecule can be employed for tuning the metal-to-metal interaction, influencing the electric and magnetic properties. This seems to be the case for 1,2,4,5-tetrazine (tz),[11] which is expected to be a stronger π acceptor than the more widely used pyrazine because of the presence of a higher number of nitrogen atoms in the ring. In fact, on this basis, one can rationalize the conductivity properties of nondoped stacked tz-bridged metallophthalocyanines and the intense intervalence transition at very low energy ($\sim$4000 cm^{-1}) in the mixed-valence form of the tz-bridged binuclear pentacyanoiron complexes.[12]

With the aim of elucidating the factors that rule the metal−metal interaction and the efficiency of the electron-transfer processes in oligonuclear species with unpaired electrons, we report here the results of an experimental and theoretical study on the $[(NH_3)_5Ru(tz)]^{2+}$ complex, a building block for the dinuclear and larger oligometallic species. This ion has been synthesized and isolated as both tetraphenylborate and perchlorate salt, and its visible photochromic behaviors have been studied using solvents that have different donor numbers, such as water, dimethyl sulfoxide (DMSO), and nitromethane (NM). The experimental data have been compared with the results of the extensive configuration-interaction (CI) calculations followed by the perturbative energy corrections, in which the solvent effects are included by an original implementation of the polarizable continuum model[13] devised in our group.[14] This allows the assignment of the observed bands in terms of transitions between a few frontier orbitals and a rationale of the solvent dependence. The agreement between theoretical and experimental spectra is substantially ameliorated going beyond the vertical approximation and taking into account the energy curves of the relevant states versus the Ru−tz bond length.

Experimental Section

Materials. $[(NH_3)_5RuCl]Cl_2$[15] and tz[16] were synthesized as reported in the literature. Solvents (HPLC grade) were used without further purification. Deionized water was distilled twice and degassed with argon before use. The following reagents were used as received: silver trifluoroacetate, sodium tetraphenylborate, lithium perchlorate (Aldrich), and trishydroxylmethylaminomethane (Trizma base, Sigma). Zinc amalgam was prepared by a standard method using granular zinc and $HgCl_2$ (Aldrich). The buffer solution at pH 8 was prepared by dissolving 3.0 g of Trizma in 250 mL of distilled water and adjusting the pH with chloridric acid. The preparation of the complexes was made under an argon atmosphere using standard Schlenk tubes; filtrations and purifications were usually performed in the air.

Spectra. IR spectra (KBr pellets) were recorded with a Perkin-Elmer 1330 IR spectrophotometer. ^{1}H NMR spectra were recorded with a Bruker AC-200 spectrometer (sodium 2,2-dimethyl-2-silapentane-5-sulfonate was the external reference for the spectra in D_2O; TMS was the internal reference for those in acetone-d_6). Visible spectra were recorded in 1 cm quartz cells with an Ultrospec 2100 pro spectrophotometer.

$[(NH_3)_5Ru(tz)](BPh_4)_2$ (1). A mixture of $[(NH_3)_5RuCl]Cl_2$ (0.200 g, 0.68 mmol) and silver(I) trifluoroacetate (0.300 g, 1.35 mmol) in water (4 mL) was digested at 80 °C until the silver chloride had coagulated. It was then cooled and filtered, and the filtrate was collected and deoxygenated with argon in a Schlenk vessel. Freshly prepared zinc amalgam (ca. 0.540 g) and an aqueous solution of tetrazine (0.300 g, 3.65 mmol in 3 mL) were added to the mixture, and the pH was adjusted to 2−3. The mixture was stirred in the dark for 1 h. The resulting solution, deep red in color, was filtered, and a buffer solution at pH 8 (15 mL) saturated with $NaBPh_4$ was added. The crude product that precipitated was filtered out and dried under vacuum. It was then purified by ion-exchange column chromatography using Sephadex CM C25 (25 cm × 3 cm) as the stationary phase; NaCl solutions of increasing molarity (from 0.2 to 0.6 M) in 3:5 $(CH_3)_2CO/H_2O$ (v:v) were used as the eluants. The deep-red fraction that eluted with NaCl (0.6 M) was collected and rotary evaporated almost to dryness. The solid mixture was extracted with methanol in order to separate the excess of NaCl that was filtered out. From the filtrate, precipitation was induced by adding a buffer solution at pH 8, saturated with $NaBPh_4$. The precipitate was collected by filtration, washed with a small portion of neutral water, and dried under vacuum. Recrystallization from acetone/ether gave 0.100 g of a red solid (0.11 mmol, 16%). Anal. Calcd for $C_{50}H_{57}N_9RuB_2\cdot 2CH_3COCH_3\cdot 3H_2O$: C, 62.45; H, 7.02; N, 11.70. Found: C, 62.80; H, 7.22; N, 11.76. Vis (H_2O, ca. 0.32 mM): 519 nm. ^{1}H NMR (acetone-d_6, TMS internal reference, ppm) δ: 9.94 (1H, d, J = 2.7 Hz, tz); 8.97 (1H, d, J = 2.7 Hz, tz); 7.33 (16H, m, BPh_4, *m*-H); 6.93 (16H, t, J = 7.1 Hz, BPh_4, *o*-H); 6.77 (8H, t, J = 7.1 Hz, BPh_4, *p*-H); 4.9 (3H, br s, *trans*-NH_3); 3.09 (12H, br s, *cis*-NH_3). IR (KBr pellet, ν/cm^{-1}): 3300, 3220, 3160 br s [ν_{NH}]; 3050, 2980 br s [ν_{CH}]; 1620 s, 1300 s [δ_{NH}].

$[(NH_3)_5Ru(tz)](ClO_4)_2$ (2). Compound **1** (0.090 g, 0.1 mmol) was dissolved in acetone (3 mL), and a saturated solution of lithium perchlorate in ethanol was added until precipitation occurred. The solid that was obtained was filtered out, washed with a small portion of ethanol, and dried under vacuum. Anal. Calcd for $C_2H_{17}N_9RuCl_2O_4\cdot 0.25CH_3CH_2OH$: C, 6.27; H, 3.89; N, 26.32. Found: C, 6.58; H, 3.98; N, 26.54. Vis (H_2O, ca. 0.32 mM): 519 nm. ^{1}H NMR (D_2O, DSS external reference, ppm) δ: 9.36 (1H, d, J = 2.4 Hz, tz); 8.69 (1H, d, J = 2.4 Hz, tz); 4.67 (3H, br s, *trans*-NH_3); 2.73 (12H, br s, *cis*-NH_3). IR (KBr pellet, ν/cm^{-1}): 3300−3160 br s [ν_{NH}]; 1620 s, 1300 s [δ_{NH}], 1100 br s [ClO_4].

Theoretical Methods and Computational Details

The absorption spectrum in the three solvents has been studied by an ab initio multireference CI approach[17] for the ground state and the two lowest singlet excited states, i.e., those involved in the two intense metal-to-ligand charge-transfer (MLCT) visible bands.

The solute−solvent interaction has been considered within the Polarizable Continuum Model (PCM)[13] that is derived by the Onsager Reaction Field model.[18] In this picture, the solvent is

(11) Kaim, W. *Coord. Chem. Rev.* **2002**, *230*, 127.
(12) (a) Glöckle, M.; Kaim, W. *Angew. Chem., Int. Ed.* **1999**, *38*, 3072. (b) Glöckle, M.; Kaim, W.; Klein, A.; Roduner, E.; Hübner, G.; Zalis, S.; van Slageren, J.; Renz, F.; Güttlich, P. *Inorg. Chem.* **2001**, *40*, 2256.
(13) Tomasi, J.; Persico, M. *Chem. Rev.* **1994**, *94*, 2027.
(14) (a) Cacelli, I.; Ferretti, A. *J. Chem. Phys.* **1998**, *109*, 8583. (b) Cacelli, I.; Ferretti, A. *J. Phys. Chem.* **1999**, *103*, 4438. (c) Cacelli, I.; Ferretti, A.; Toniolo, A. *J. Phys. Chem. A* **2001**, *105*, 4480.
(15) Chang, J. P.; Fung, E. Y.; Curtis, J. C. *Inorg. Chem.* **1986**, *25*, 4233 and references therein.
(16) (a) Marcelis, A. T. M.; van der Plas, H. C. *J. Heterocycl. Chem.* **1987**, *24*, 545. (b) Sauer, J.; Heldmann, D. K.; Hetzenegger, J.; Krauthan, J.; Sichert, H.; Schuster, J. *Eur. J. Org. Chem.* **1998**, 2885.
(17) (a) Cimiraglia, R. *J. Chem. Phys.* **1985**, *83*, 1746. (b) Angeli, C.; Cimiraglia, R.; Persico, M.; Toniolo, A. *Theor. Chem. Acc.* **1997**, *98*, 57.
(18) Onsager, L. *J. Am. Chem. Soc.* **1936**, *58*, 1486.

modeled by an infinite continuum medium (with a dielectric constant ϵ) outside a polyhedral cavity surrounding the solute molecule. The electronic distribution of the solute polarizes the solvent inducing a charge distribution on the cavity surface, which originates a reaction field potential V that must be added to the electrostatic Hamiltonian in a vacuum H_0. Thus, the nonlinear Schrödinger equation to be solved is

$$[H_0 + V(\epsilon,\rho_0)]|\Psi_a\rangle = E_a|\Psi_a\rangle \quad (1)$$

The potential V in eq 1 depends on the dielectric constant ϵ, the shape of the cavity, and the density function ρ_0 of the ground state Ψ_0. In principle, each of the electronic states Ψ_a of the solute can induce a different polarization on the cavity surface. However, in a fast photon absorption process, we assume that the sudden excitation from the ground state does not allow the surrounding solvent molecules to relax, and we can use the surface charge distribution, arising from ρ_0, to build the reaction field for all of the considered electronic states.[14]

We assume, as for the pyrazine and bipyridine pentaammine ruthenium complexes that have been so far investigated,[14] that the main source of solute−solvent interaction is the formation of the hydrogen bonds between the solvent and the ammonia ligand. Each ammonia−solvent hydrogen bond increases the electron density on the ammonia N and thus, reinforcing its electron-donor capability, affects the charge distribution on both the metal and the aromatic ligand. Because the PCM method is based on a classical description of the solute−solvent electrostatic interaction, quantum effects cannot be properly taken into account. On the other hand, a good description of the metal-to-ligand absorption process requires an accurate estimate of the electron density around the metal. In a previous paper,[14] we demonstrated that, because the Ru atom is far enough from the solute−solvent interface, quantum H-bonding effects can be accurately simulated by a suitable choice of the cavity. The width of the cavity surrounding the ammonia is chosen by a comparison of the electronic density around the metal, computed for a simplified solute−solvent supermolecule, with that obtained by PCM calculations with different spheres around NH_3. This is carried out under the assumption that the overall solvent effect on the metal results from almost independent contributions of each ammonia as well as of other ligands. According to ref 14a, the optimized cavity radii for ammonia were 1.82, 1.72, and 1.67 Å for NM, H_2O, and DMSO, respectively. These radii are used in the present paper. This approach, however, does not allow the investigation of the solvent−solute electron-transfer process that has been reported in the literature.[19]

The best single determinant is obtained by a PCM−SCF-HF (SCF-HF = self-consistent-field, Hartree−Fock) calculation with a 6-31G basis set and the 36-electron effective core potential (ECP) of Hay and Wadt for ruthenium,[20] using the GAMESS package.[21] The integrals, including the one-electron reaction field matrix, have then been transformed from an atomic to a molecular basis. When we froze the 1s orbital of the N and C atoms and discarded the unoccupied orbitals with energy above a given threshold, the selected orbital subspace utilized in the CI calculations included 39 occupied and 40 empty SCF orbitals.

The multireference CI computational sequence is based on the configuration interaction by perturbation with a multiconfigurational zero-order wave function selected iteratively (CIPSI) method[22] and is organized into four sequential steps where the CI space is gradually enlarged by using the aimed selection procedure. At the beginning, a configuration space W_0 is defined including the SCF determinant and some single excitations that reasonably contribute to the excited states of interest. The ground and desired excited states are then obtained at this level of approximation ("zero-order" states) diagonalizing the Hamiltonian in this space. The space $W_P = W_S + W_D$ is then built, where W_S and W_D are the determinants with single and double excitations from W_0. Using the first-order perturbative correction of each determinat to the "zero-order" states, a subspace W_η of W_P is selected so that the norm of the first-order correction is equal to a given value η. The space W_η is then added to W_0, and the new updated "zero-order" states can be computed. The whole sequence is then repeated until a reasonable compromise between the level of accuracy and the computational effort is reached. It should be stressed that η is kept the same for all of the desired states and solvents; this provides a balanced description of the ground and excited states, which is of primary importance in evaluating the excitation energies from the difference of the absolute energies. The final variational energies of both the ground and excited states are then corrected by second-order diagrammatic perturbation[17] using the Epstein−Nesbet partition scheme. In this step, the perturbative contributions of the single and double excitations of all Slater determinants belonging to the final W_0 configurational space (~4000 detors) are considered (more than 2×10^6 contributions).

To calculate the line-shape profile of the bands, one must take into account the dependence of the energy of the ground and excited states, involved in the lowest transitions, on the Ru−N(tetrazine) bond length. Therefore, calculations have been performed at several values of the Ru−N(tetrazine) distance within the Franck−Condon region, and the vibrational wave functions pertaining to this coordinate have been computed and used to evaluate the line-shape profile of the relevant electronic transitions. The necessity of going beyond the vertical-transition approximation is related to the change in the nature of the lowest excited states and will be discussed in the next sections.

The vibrational eigenvalue equation for the Ru−N(tetrazine) distance (called R from now on in this section) for the electronic state Ψ_K with potential energy $V_K(R)$, in the Born−Oppenheimer approximation, is

$$\left[-\frac{1}{2\mu}\frac{d^2}{dR^2} + V_K(R)\right]\chi_{\upsilon K}(R) = E_{\upsilon K}\chi_{\upsilon K}(R) \quad (2)$$

where υ is the vibrational quantum number and μ is the reduced mass. The latter has been computed by considering this motion as arising from a diatomic, i.e., $1/\mu = 1/M_{Ru} + 1/M_N$, where M_{Ru} and M_N are the masses of the Ru(NH$_3$)$_5$ and tz fragments, respectively. It is clear that R does not have a precise correspondence with any normal coordinate of the molecule; rather, it is the local internal coordinate that embodies the different potential energy of the first electronic states. For states lying in the vibrational continuum, the index υ becomes the energy E_K of the vibrational state and can

(19) (a) Stavrev, K. K.; Zerner, M.; Meyer, T. J. *J. Am. Chem. Soc.* **1995**, *117*, 8684. (b) Pearl, G. M.; Zerner, M. *J. Am. Chem. Soc.* **1996**, *118*, 2059.

(20) (a) Hay, P. J.; Wadt, W. R. *J. Chem. Phys.* **1985**, *82*, 270. (b) Hay, P. J.; Wadt, W. R. *J. Chem. Phys.* **1985**, *82*, 284. (c) Hay, P. J.; Wadt, W. R. *J. Chem. Phys.* **1985**, *82*, 299.

(21) (a) Schmidt, M. W.; Baldridge, K. K.; Boats, J. A.; Elbert, S. T.; Gordon, M. S.; Jensen, J. H.; Koseki, S.; Matsunaga, N.; Nguyen, K. A.; Su, S. J.; Windus, T. L.; Dupuis, M.; Montgomery, J. A. *J. Comput. Chem.* **1993**, *14*, 1347. (b) Mennucci, B.; Toniolo, A.; Cappelli, C. *J. Chem. Phys.* **1999**, *111*, 7197.

(22) (a) Cimiraglia, R. *J. Chem. Phys.* **1985**, *83*, 1746. (b) Angeli, C.; Cimiraglia, R.; Persico, M.; Toniolo, A. *Theor. Chem. Acc.* **1997**, *98*, 57. (c) Angeli, C.; Persico, M. *Theor. Chem. Acc.* **1997**, *98*, 117.

take any value higher than the asymptotic energy $V_K(\infty)$, while the wave functions have to be normalized to an energy Dirac δ function.

Consistently with the eigenvalue equation, the $V_K(R)$ energies are computed, leaving the geometry of the two fragments unchanged. This is of course a rather crude approximation, which neglects the nuclear relaxation (different for each electronic state) following the scan of the active coordinate R. Nevertheless, a state-by-state geometry optimization is not easily feasible and, furthermore, it would lead to relevant difficulties in evaluating the Franck−Condon factors because of their dependence on all of the internal coordinates. Thus, the present choice can be considered a reasonable compromise in which all of the electronic states are treated on equal footing.

The absorption cross section (in units of a_0^2) for the photon energy ω (in bohr) is

$$\sigma_K(\omega) = 2\pi^2 \alpha a_0^2 \left[\sum_v f_{vK} \delta(\omega - \omega_{vK}) + g_K(\omega) \right] \tag{3}$$

where $\omega_{vK} = E_{vK} - E_{00}$, the f_{vK} is the oscillator strength for a transition to the discrete states, and $g_K(\omega)$ is the oscillator strength density for states in the continuum, which vanishes for ω in the discrete region. α is the fine structure constant ($\approx 1/137$), and a_0 is the Bohr radius. In practical calculations, the Dirac δ functions have been substituted by sharp normalized Gaussians. The oscillator strengths and oscillator strength density are respectively

$$f_{vK} = \frac{2}{3} \left| \int \mathrm{d}R\, \chi^*_{00}(R)\, T_{0K}(R)\, \chi_{vK}(R) \right|^2 \tag{4a}$$

$$g_K(\omega) = \frac{2}{3} \left| \int \mathrm{d}R\, \chi^*_{00}(R)\, T_{0K}(R)\, \chi_{\epsilon K}(R) \right|^2 \tag{4b}$$

where the energies ω and ϵ are related by $\omega + E_{00} = \epsilon + V_K(\infty)$. Thus, the absorption intensity from the vibronic ground state $|\chi_{00}\Psi_0\rangle$ to the state $|\chi_{vK}\Psi_K\rangle$ arises from the integration along the active coordinate R of the electronic-transition moment weighted by the product of the vibrational wave functions. The electronic-transition moments are computed in the mixed length−velocity gauge, which makes f_{vK} and $g_K(\omega)$ independent from the transition energy, as

$$T^2_{0K}(R) = \langle \Psi_0 | \vec{r} | \Psi_K \rangle \cdot \langle \Psi_K | \vec{\nabla} | \Psi_0 \rangle \tag{5}$$

where $\vec{r}$ and $\vec{\nabla}$ are the length and velocity dipole operators acting on the electronic coordinates, respectively, and the dependence of the electronic wave functions on R has been omitted for simplicity.

The total photoabsorption cross section, obtained by summing over the electronic states $\sigma(\omega) = \sum_K \sigma_K(\omega)$, is related to the absorbivity ϵ (in $\mathrm{M^{-1}\ dm^{-1}}$) by

$$\epsilon(\omega) = \sigma(\omega)\, N_A \times 10^{-20} \tag{6}$$

where σ is to be expressed in Mbarn (1 Mb $= 10^{-18}$ cm^2) and N_A is the Avogadro number. Finally, the absorbance can be evaluated by the usual formula

$$A(\omega) = \epsilon(\omega)\, CL \log e \tag{7}$$

in which C is the concentration in mol/dm^3 and L is the optical path in dm.

Results and Discussion

Synthesis and Characterization. The preparative procedure has been based on the reduction of $[Ru(NH_3)_5(H_2O)]^{3+}$ with zinc amalgam in the presence of the ligand, which is a largely applied method for the synthesis of mononuclear[23] and oligonuclear[23b,24] ruthenium(II) polyammine complexes.

Unfortunately, the yield of the desired product is very low (18% after purification by ion-exchange chromatography), and at least three more species are formed that can be eluted from the column at increasing ionic strength. One of them, green in color, has been identified as the dinuclear complex $[\{Ru(NH_3)_5\}_2(\mu\text{-tz})]^{4+}$ by comparison of its elemental and spectroscopic data with those of an X-ray structurally characterized sample, which we were able to prepare in fairly good yields.[25]

Owing to the presence of three noncoordinated nitrogen atoms, the mononuclear complex can obviously behave as a base; in order to obtain the salts of the unprotonated complex, the precipitations were performed in controlled pH conditions; otherwise, mixtures of unprotonated and protonated species were obtained. BPh_4^- and ClO_4^- were employed as counteranions that gave rise respectively to salts soluble in either organic solvents (**1**) or water (**2**). They are stable in air as both solids and solutions.

The ^{1}H NMR spectrum of **1** in acetone-d_6 exhibits an AB pattern in the aromatic region, consisting of two doublets with an intensity ratio of 1:1; in the range of 3−5 ppm, two signals are observed whose integrals account for four ammonia groups trans and one cis to the tetrazine ring. The intensity of the tetraphenylborate signals is fully consistent with the net charge of the complex. The ^{1}H NMR spectrum of **2** in D_2O confirms the above assignments; a H/D exchange is observed for ammonia groups with the progressive disappearance of their signals, which is complete in 1 day at room temperature.

IR spectra show the expected strong absorption maxima in the range of 3300−3140 cm^{-1} [ν_{NH}], 1620 s, and 1300 s [δ_{NH}]. In the deuterium-exchanged species, these bands move to 2440−2300, 1200, and 1000 cm^{-1}, respectively.

The cyclic voltammetry of **2** (ca. 1×10^{-3} M in a 0.1 M sodium perchlorate aqueous solution) shows a totally irreversible process with an anodic peak at $E = 0.918$ V (versus Ag/AgCl electrode), attributable to the oxidation of the metal center immediately followed by the complex decomposition, as demonstrated also by the spectroelectrochemical measurements that exhibit a progressive disappearance of the visible bands during the electrolysis. The instability of the oxidized complex is probably related to the insufficient back-donation from a too electron-poor $[Ru(NH_3)_5]^{3+}$ center to the otherwise strong π-acceptor tetrazine ring.

Ground-State Geometry Optimization. The geometry of the complex has been optimized at the density functional

(23) (a) Ford, P. C.; Rudd, D. F. P.; Gaunder, R. G.; Taube, H. *J. Am. Chem. Soc.* **1968**, *90*, 1187. (b) Creuz, C.; Taube, H. *J. Am. Chem. Soc.* **1973**, *75*, 1086. (c) Curtis, J. C.; Sullivan, B. P.; Meyer, T. J. *Inorg. Chem.* **1983**, *22*, 224.

(24) (a) von Kameke, A.; Tom, G. M.; Taube, H. *Inorg. Chem.* **1978**, *17*, 1790. (b) Sommovigo, M.; Ferretti, A.; Venturi, M.; Ceroni, P.; Giardi, C.; Denti, G. *Inorg. Chem.* **2002**, *41*, 1263.

(25) Denti, G.; et al., manuscript in preparation. It is noteworthy that W. Kaim and co-workers recently reported (ref 12b) that all of their attempts to obtain that species failed "presumabily because of proton-coupled electron-transfer reaction of the extremely reducible tz heterocycle".

Table 1. Relevant Ru−N Bond Distances of the Ground-State Geometry Optimized at the DFT Level

bond	value (Å)
Ru−N_{tz}	1.99 (NM), 1.97 (DMSO, H_2O)
Ru−NH_3, cis	2.18,[a] 2.20
Ru−NH_3, trans	2.21

[a] NH_3 groups near to *o*-N with respect to the Ru−tz bond.

theory (DFT) level of theory using the widely used B3LYP functional[26] and including the solute−solvent interaction through the PCM method. The cavity surrounding the solute was modeled by the above-reported solvent-specific radii (1.82, 1.72, and 1.67 Å for NM, H_2O, and DMSO, respectively) for the spheres on the five NH_3 groups and standard solvent-independent spheres for the remaining part of the molecule.[27] All of the calculations were carried out by the Gaussian 98 package[28] using the 6-31G* one-electron basis with ECP on Ru.[20]

As expected, the aromatic ring takes a nearly planar conformation; four Ru−NH_3 bonds form angles of about 45° with this plane, and the fifth Ru−NH_3 bond forms an angle of about 180° with the Ru−N_{tz} bond. The Ru−N bond distances in the ground state optimized in the three solvents are summarized in Table 1. Owing to the back-bonding effect involving the metal d orbitals and the aromatic low-lying empty π^* orbitals, the Ru−N_{tz} distance is smaller than the Ru−NH_3 one. Although the optimized geometry does not show abrupt variations with the solvent, at least for the three considered here, the Ru−N_{tz} distance appears to be slightly larger in NM. Because the in vacuo calculations yield even larger Ru−N_{tz} values, this feature can be related to the solvent, which pushes the electronic charge toward the metal and thus increases the metal-to-ligand back-bonding. Therefore, solvents with large donor numbers such as DMSO and H_2O are expected to reinforce the Ru−N_{tz} linkage, which results in shorter bond lengths.

Because no structure is available from the literature and we have been unable to obtain crystals of suitable dimensions for X-ray diffraction, a comparison with the experimental data cannot be done. While the Ru−NH_3 distances are very similar to those of other $[(NH_3)_5Ru-L]^{2+}$ complexes,[29] the Ru−aromatic ligand equilibrium distance is slightly smaller than that observed for L = pyrazine, where it was found to be 2.006 Å in the crystalline phase.[29] Although a direct comparison between the geometries in the crystalline phase and in solution is not straightforward, this finding may be in line with the expected enhancement of the back-bonding interaction because of the two low-lying empty π^* orbitals of tetrazine.

Experimental Absorption Spectra of $[(NH_3)_5Ru(tz)]^{2+}$. The absorption spectra of a 0.32 mM solution of the $[(NH_3)_5Ru(tz)]^{2+}$ complex in NM, water, and DMSO are reported in Figure 1. The spectra are in all cases characterized by a broad band in the visible spectrum at ∼2.3 eV and a marked shoulder above 3.0 eV. The spectrum for the NM solution shows additional features at 3.6−3.8 eV, but because this region is affected by solvent absorption, these are of little significance. To identify the single absorption bands, a fitting with two or three (for NM) Gaussian functions was performed; the results are summarized in Table 2.

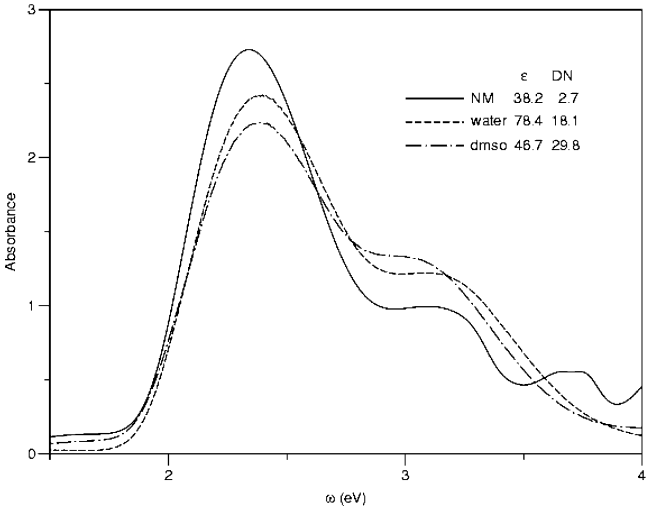

Figure 1. Absorption spectra of $[(NH_3)_5Ru(tz)]^{2+}$ (0.32 mM) in NM, water, and DMSO. The optical path is 1 cm.

Table 2. Visible Spectral Data for $[(NH_3)_5Ru(tz)]^{2+}$ in Different Solvents[a]

			first band		second band	
solvent	DN	ϵ^b	ω_{max} ($\epsilon \times 10^{-3}$)[c]	W, B[c]	ω_{sh} ($\epsilon \times 10^{-3}$)[d]	W, B[d]
NM[e]	2.7	38.2	2.32 (7.87)	0.44, 1.38	2.98 (3.12)	0.86, 1.08
water	18.1	78.4	2.36 (6.81)	0.46, 1.27	3.05 (3.84)	0.83, 1.27
DMSO	29.8	46.7	2.33 (5.68)	0.46, 1.05	2.97 (4.09)	0.85, 1.40

[a] Photon energy (ω) in eV and molar absorbivity (ϵ) in $cm^{-1}\,M^{-1}$. Two-Gaussian fit for water and DMSO and three-Gaussian fit that includes the 3.77 eV band for NM. [b] Dielectric constant. [c] Parameters of the Gaussian fit for the band: $A(\omega) = (B/W)\sqrt{2/\pi}e^{-2(\omega-\omega_{max})^2/W^2}$. [d] Same as in footnote *c* for the shoulder (ω_{sh}) instead of ω_{max}. [e] The parameters for the third Gaussian function used in this case are $\omega = 3.77$, $W = 0.26$, and $B = 0.13$.

Although similar species, such as the $[(NH_3)_5Ru-pyrazine]^{2+}$ system, show a significant red shift as the Gutman donor number (DN) of the solvent increases,[14a,30] in this case, the position of the two bands is stable with the solvent. However, the solvent is seen as affecting the relative intensities of the two bands; the intensity of the low-energy band decreases with increasing DNs, while the opposite occurs for the shoulder at higher energy. Because the overall intensity of the two bands is about constant, it appears that solvents characterized by a large DN move some spectral weight from the low to the high energy band. It is worth noticing that for the system under study, as well as for similar complexes previously studied,[14,19,31] the effects of the solvents considered on the molecular absorption spectrum cannot simply be related to the dielectric constant but rather to the electron donor strength expressed by the empirical DN.

Theoretical Absorption Spectra. The two observed bands can be interpreted as MLCT transitions, in which a fraction

(26) Becke, A. D. *J. Chem. Phys.* **1993**, *98*, 5648.
(27) Barone, V.; Cossi, M.; Tomasi, J. *J. Chem. Phys.* **1997**, *107*, 3210.
(28) Frisch, M. J.; et al. *Gaussian98*.
(29) Gress, M. E.; Creutz, C.; Quicksall, C. O. *Inorg. Chem.* **1981**, *20*, 1522.
(30) Creutz, C.; Chou, M. H. *Inorg. Chem.* **1987**, *26*, 2995.

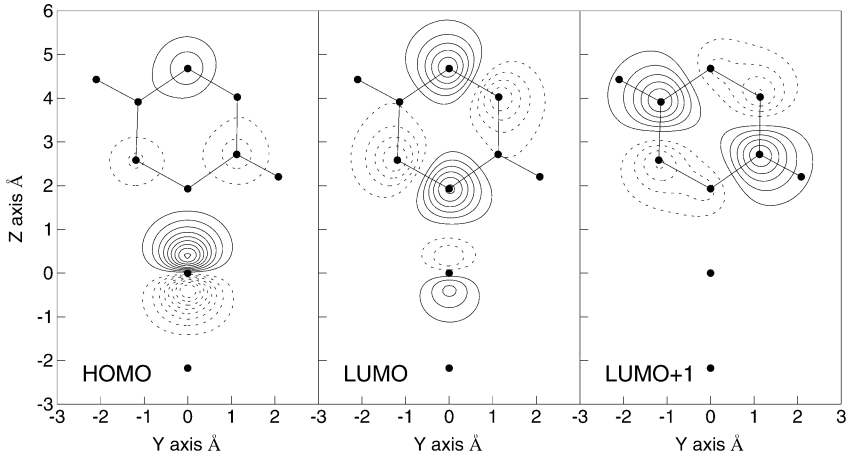

Figure 2. Map of the low-lying orbitals involved in the MLCT transitions (in water). The value of the *x* coordinate is 0.6 Å. Full and dashed lines indicate the lobes with different signs.

of electronic charge is transferred from the metal to the aromatic ligand. Within a monoelectronic picture, the related excited states correspond to the single excitations in which one electron is promoted from a doubly occupied metal-centered d orbital, the HOMO (H), to the two lowest ligand-based π^* orbitals, LUMO (L0) and LUMO+1 (L1). Because the ligand ring was taken in the *yz* plane with the metal−ring direction along the *z* axis, the involved metal d orbital is the d_{xz}, in analogy with $Ru(NH_3)_5$ complexes with other N-aromatic ligands.

A section of these three orbitals (in a plane parallel to the *yz* plane at a distance of 0.6 Å) is reported in Figure 2 for the complex in water. The maps confirm that both the H → L0 and H → L1 transitions should lead to consistent charge transfer from the metal to the aromatic ligand. The figure shows that L0 has a relevant charge distribution on the N atoms, while L1 is essentially localized on the C−H bonds with minor lobes on the N−N aromatic bonds. The density on the N atom close to Ru, which is much larger in L0 than in L1, suggests that the H → L0 transition may be stronger than the H → L1 transition. The main component of both the transition moments $\langle H|T|L0\rangle$ and $\langle H|T|L1\rangle$, where T is the dipole transition operator, is expected along *z*, although a smaller contribution may come from *y*.

The presence of two bands, interpreted as H → L0 and H → L1 transitions, originates from the presence of four nitrogens in the tz ligand that breaks the symmetry with respect to the reflection plane *xz* and enables both of the two lowest π^* orbitals to have a component in the $Ru-N_{tz}$ region. This is different from the spectrum observed for similar Ru complexes with aromatic μ ligands with one or two nitrogen atoms (e.g., pyridine and pyrazine), where the *xz* symmetry plane is preserved (approximate C_{2v} symmetry). In this case, one of the two π^* orbitals is antisymmetric for the reflection in the *xz* plane and must have null density in the $Ru-N_{tz}$ region. Although it is symmetry-allowed, the corresponding $d_{xz}-\pi^*$ transition takes a small value in the *z* component. The same holds as far as the *y* polarization of the same transition is concerned; it is allowed in principle, but the different spatial distributions of the two orbitals make the oscillator strength very small. Actually, only one transition is seen in the experimental spectrum.

This simple one-electron picture may help in the rationalization of the origin of the observed bands, but in order to reach the quantitative comparison between the experimental and theoretical results, more refined computational methods are necessary. Unfortunately, even including the electronic correlation and relaxation effects by multireference CI calculations, the results obtained at the optimized equilibrium geometry do not properly account for the observed intensities of the bands, especially for water and NM. In addition, it would be of great interest to have the theoretical estimates of the line-shape profile in order to get a better comparison with the experimental spectra of Figure 1.

We then explored the dependence of the ground and two lowest singlet excited states on the $Ru-N_{tz}$ bond coordinate, because this is the internal degree of freedom that can be expected as the most involved in the metal-to-ligand electron transfer. We performed a series of CI calculations for different values of the $Ru-N_{tz}$ distance ($R_{Ru-N_{tz}}$), keeping all of the remaining internal coordinates fixed at their optimized value. This will also enable the calculation of the line-shape profile of the two bands.

For values of $R_{Ru-N_{tz}}$ ranging from 1.80 to 2.06 Å, the shapes of the three orbitals H, L0, and L1 do not change appreciably. On the contrary, at the CI level, while the ground state (S_0) is roughly found to be essentially the SCF ground state ($|^1\phi_0\rangle$), the composition of the two lowest spin singlet excited states (S_1 and S_2) in terms of the single excited H → L0 ($|^1\phi_{L0}\rangle$) and H → L1 ($|^1\phi_{L1}\rangle$) spin singlet configurations is seen to change drastically with $R_{Ru-N_{tz}}$. In particular, for values of $R_{Ru-N_{tz}}$ close to the minimum in the ground state, the two excited states exchange their basic configuration with each other as the result of an avoided crossing. This is clearly seen after writing the ground state S_0 and the two lowest

(31) (a) Shin, Y. K.; Brunschwig, B. S.; Creutz, C.; Newton, M. D.; Sutin, N. *J. Phys. Chem.* **1996**, *100*, 1104. (b) Sizova, O. V.; Baranovski, V. I.; Ivanova, N. V.; Panin, A. I. *Russ. J. Coord. Chem.* **1998**, *24*, 219. (c) Zeng, J.; Hush, N. S.; Reimers, J. R. *J. Am. Chem. Soc.* **1996**, *118*, 2059. (d) Zeng, J.; Hush, N. S.; Reimers, J. R. *J. Phys. Chem.* **1996**, *100*, 19292. (e) Hush, N. S.; Reimers, J. R. *Coord. Chem. Rev.* **1998**, *177*, 37. (f) Hush, N. S.; Reimers, J. R. *Chem. Rev.* **2000**, *100*, 775.

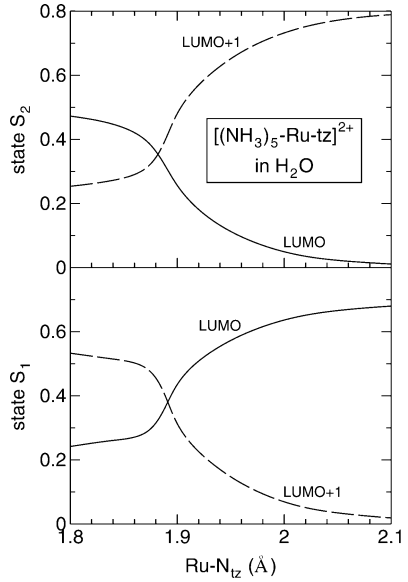

Figure 3. Excited states S_1 and S_2 decomposed according to eq 8 (see text). The weight of the $|^1\phi_{L0}\rangle$ (H → L0) and $|^1\phi_{L1}\rangle$ (H → L1) configurations is reported for the two states as a function of the Ru−N_{tz} distance.

spin singlet excited states S_1 and S_2 as a linear combination of the relevant configurations as

$$|S_0\rangle = C_0^0|^1\phi_0\rangle + C_{L0}^0|^1\phi_{L0}\rangle + C_{L1}^0|^1\phi_{L1}\rangle + \sum_M C_M^0|^1\phi_M\rangle$$

$$|S_1\rangle = C_0^1|^1\phi_0\rangle + C_{L0}^1|^1\phi_{L0}\rangle + C_{L1}^1|^1\phi_{L1}\rangle + \sum_M C_M^1|^1\phi_M\rangle$$

$$|S_2\rangle = C_0^2|^1\phi_0\rangle + C_{L0}^2|^1\phi_{L0}\rangle + C_{L1}^2|^1\phi_{L1}\rangle + \sum_M C_M^2|^1\phi_M\rangle \quad (8)$$

and plotting $|C_{L0}^1|^2$, $|C_{L0}^2|^2$, $|C_{L1}^1|^2$, and $|C_{L1}^2|^2$ as a function of $R_{Ru-N_{tz}}$, as shown in Figure 3 for the computations in water. It is clear that, for small values of $R_{Ru-N_{tz}}$, S_1 is basically a H → L1 excitation and gradually turns to a H → L0 excitation as $R_{Ru-N_{tz}}$ increases. The opposite occurs for S_2. Notice that the sum of the two curves in Figure 3 shows that the contribution of the other terms of eq 8 (that in the sum over *M*) is small in all cases.

According to the above discussion, the transition moment $\langle H|T|L0\rangle$ is greater than $\langle H|T|L1\rangle$, and we expect that the more the excited state of H → L0 is in nature, the larger the oscillator strength is for the corresponding transition from the ground state. These qualitative considerations about the connection between the nature of the two lowest singlet excited states and the intensities of the resulting bands are confirmed by the computation of the transition moments for different values of $R_{Ru-N_{tz}}$.

In Figures 4, 5, and 6, for NM, water, and DMSO, respectively, we report the adiabatic energy curves of the ground and MLCT excited states, as well as the $S_0 \rightarrow S_1$ and $S_0 \rightarrow S_2$ transition moments (T_{01} and T_{02}; see eq 5), as a function of the active coordinate $R_{Ru-N_{tz}}$. The theoretical absorbances, as computed by eqs 3−7, and experimental absorbances of Figure 1 are also reported in the same figures for comparison. The amplitude of the ground vibrational state

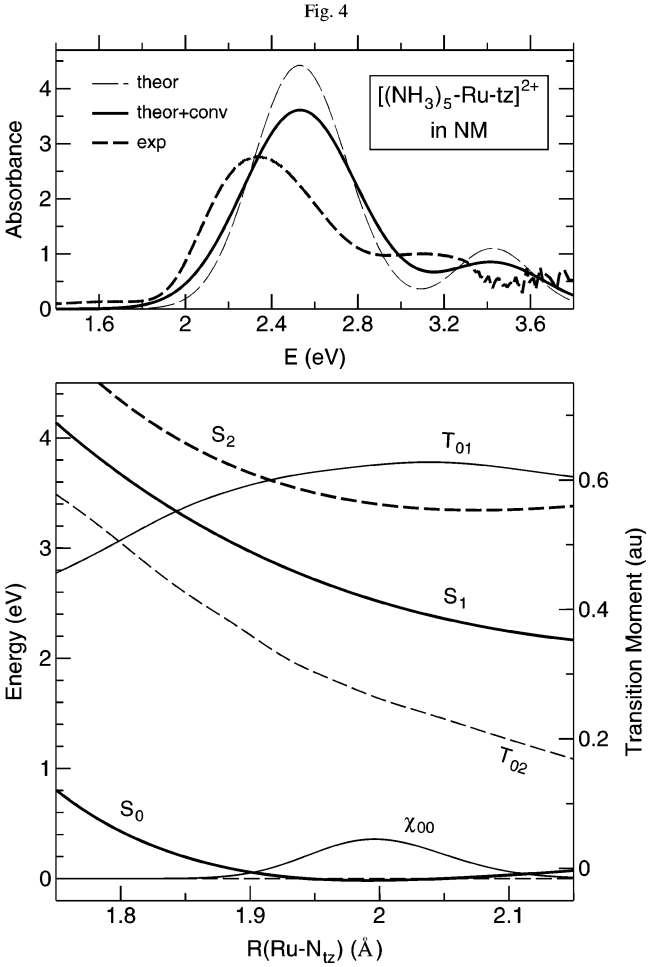

Figure 4. Comparison between the theoretical and experimental spectra in NM. In the lower panel, the ground (S_0) and the two lowest excited states (S_1 and S_2) are reported as a function of the Ru−N_{tz} coordinate (left scale) together with their corresponding transition moment (T_{01} and T_{02}) from S_0 (right scale). The zero of the left ordinate scale corresponds to the energy of the lowest vibrational level of S_0 whose wave function χ_{00} is also reported (arbitrary units). The upper panel reports the original theoretical spectrum (theor) and that obtained by a convolution with a Gaussian function with fwhm = 0.36 eV (theor + convol), together with the experimental spectrum. All absorbances refer to a 0.32 mM solution and an optical path of 1 cm.

of S_0 (χ_{00}) is also shown to delineate the Franck−Condon region and to rationalize the resulting absorption spectra as resulting from both the excitation energies and the transition moments of the two excited states (see eq 4). To account for the other sources of line broadening (internal coordinates other than $R_{Ru-N_{tz}}$ and solute−solvent coordinates) and to allow an easier comparison with the experimental absorbance, the original theoretical band profiles are convoluted with a Gaussian function with a phenomenological full width at half-maximum (fwhm) of 0.36 eV. Although no crossing between the two MLCT energy curves is put in evidence of the investigated $R_{Ru-N_{tz}}$ range, according to the preliminary indications given by Figure 3, the transition moments of the two MLCT excitations do cross each other. The fact that the transition moment T_{01} grows to the detriment of T_{02} is a clear consequence of the change of the two excited states with $R_{Ru-N_{tz}}$. It appears that the crossing point changes in position with the solvent and in particular moves to higher

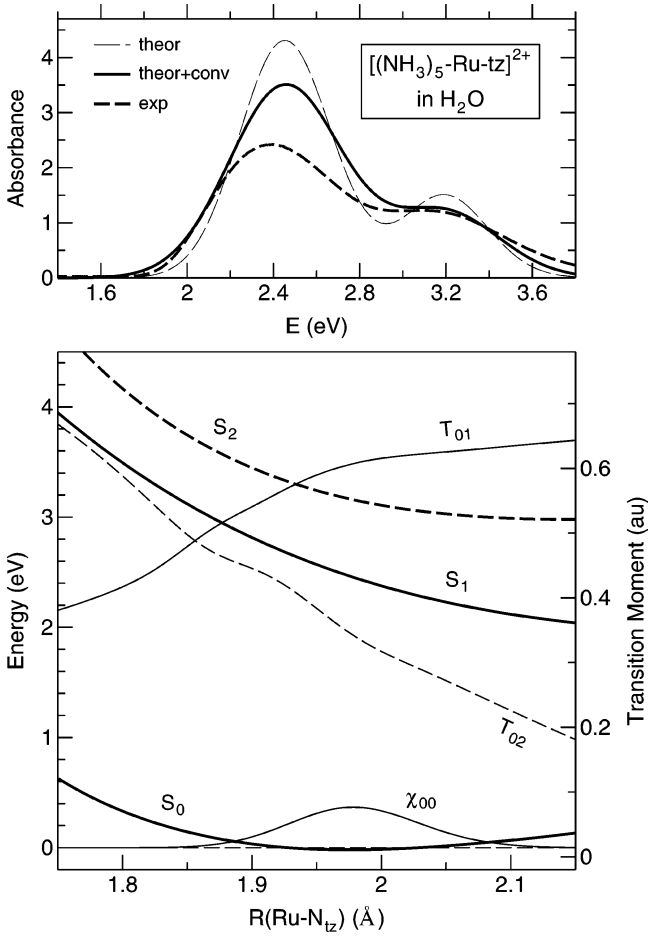

Figure 5. Same as Figure 4 for water.

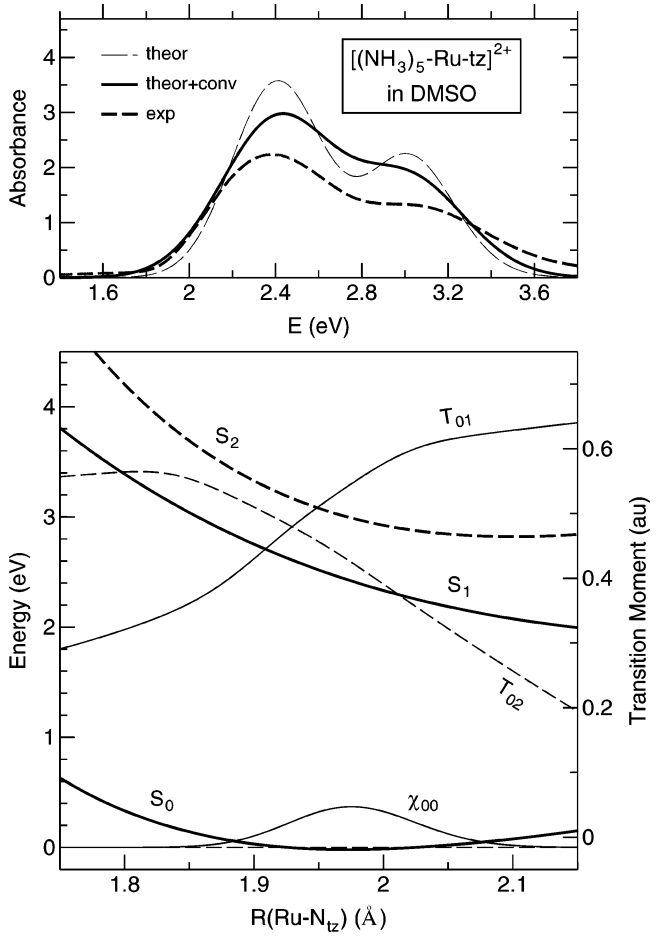

Figure 6. Same as Figure 4 for DMSO.

$R_{Ru-N_{tz}}$ values as the solvent DN increases. Because the position of the Franck−Condon region slightly changes with the solvents, the nature of S_1 and S_2 in this region depends on the solvent and explains the relative intensities of the two bands in the three solvents. For instance, in the case of NM (Figure 4) around the energy minimum of S_0 (1.99 Å), we observe $S_1 \approx H \rightarrow L0$ and $S_2 \approx H \rightarrow L1$, with the $S_0 \rightarrow S_1$ transition being by far the most intense. On the contrary, for DMSO (Figure 6), the crossing occurs around 1.92 Å, and near the energy minimum of S_0 (1.97 Å), the $H \rightarrow L0$ contribution is completely shared in both of the excited states. As a consequence, in this case, the two bands are of comparable intensity. These observations are in accordance with the experimental absorbance.

The ratio of the two bands in the theoretical absorbance is in an overall agreement with the experimental profile, although the theory predicts a slightly higher intensity of both bands in all of the three solvents. In particular, the correct sequence of the intensity ratio between the two bands with the solvent DN is correctly reproduced by the calculation. By considering the high sensitivity of the transition moments on the details of calculation, these results can be considered very satisfactory. For DMSO, the position of the first band is in very good agreement with experimental results, whereas for water and NM, the theory predicts band maximas of 0.1 and 0.3 eV higher, respectively. Therefore, the first theoretical band shows a small red shift, monotonic with DN, which is not observed in the experimental spectrum. A similar trend is also observed for the second band.

From Figures 4−6, it is apparent that for all of the solvents the energy curves of S_1 and S_2 show a different slope in the Franck−Condon region. The reorganization energy, defined as the vertical energy minus the energy at the minimum, is >0.3 eV for S_1 and ~ 0.1 eV for S_2. Because of the freezing of the internal coordinates other than $R_{Ru-N_{tz}}$, these values are probably underestimated. The calculations also predict the equilibrium geometries of the excited states at longer bond lengths. Although the employed theoretical method is not exactly size consistent, we are confident that this finding is reliable because, for small changes of the active coordinate, the aimed selection method can safely supply the lack of size consistency. Moreover, this is in line with the maps in Figure 2, where it appears that H and L1 are practically nonbonded orbitals whereas L0 appears to show small antibond character. Therefore, the considered excited states, in which L0 is partially populated, are expected to weaken the $Ru-N_{tz}$ bond.

Conclusions

We have reported an experimental and theoretical study of the $[(NH_3)_5Ru(tz)]^{2+}$ ion, which is a precursor for the preparation of oligonuclear species that are expected to

exhibit an efficient intramolecular electron transfer and thus is of significant interest in molecular electronics.

The complex has been synthesized for the first time and fully characterized. Its absorption spectrum in the visible spectrum, which has been studied in three solvents with different donor numbers, reveals the unexpected presence of two distinct MLCT bands.

Theoretical calculations, performed at the CI level and including the effects of solute−solvent interactions by means of a modified PCM approach, are consistent with the experiments and explain the observed intensities of the bands in the various solvents.

A good agreement between theory and experiment requires that the dependence of the energy of the relevant states on the Ru−tz coordinate be explicitly taken into account. Whereas computed excitation energies and intensities of the bands appear to be very sensitive to small displacements along this coordinate, the experiments show that the solvent donor number has a significant effect on the relative intensities of the two MLCT bands with minor effects on their position. These two observations suggest that efforts must be in place for theoretical approaches to properly consider the effects of the metal−ligand internal coordinate and, more importantly, that environmental effects, which may be stronger than solvation and that affect the metal−ligand equilibrium distance, can modulate the relative intensities of the two bands in the visible spectrum.

The information gained in the present work for the mononuclear compound will be useful to approach the more interesting dinuclear compound, whose study is in progress in our laboratory.

Acknowledgment. The financial support of the Italian Ministry for Education, University, and Research (Cofin 2001 project) is gratefully acknowledged.

IC034786O